Structural Effects on Adsorption of Atmospheric Gases in Mixed Li,Ag–*X*-Zeolite

Nick D. Hutson and Ralph T. Yang
Dept. of Chemical Engineering, University of Michigan, Ann Arbor, MI 48109

Silver is known to strongly affect the adsorptive properties of zeolites. In the synthesis of mixed Li,Ag low-silica X-type (LSX) zeolite, adding very small amounts of silver and specific dehydration conditions results in a sorbent with enhanced adsorptive characteristics for air separation. The location of the extraframework silver in relation to the aluminosilicate framework is of primary importance for elucidating the effect of silver cations on the adsorptive characteristics of the zeolite. In this work, mixed Li,Ag ion-exchanged zeolites were synthesized and treated to promote the formation of intracrystalline silver clusters. These samples were structurally characterized using Rietveld refinement of neutron powder diffraction data. Structural characterization revealed the presence of cations in a novel site II in mixed Li,Ag − LSX zeolites that were vacuum-dehydrated at 450°C. Cations in this site II* are more interactive with the atmospheric sorbates of interest than silver at the conventional site II location. Vacuum dehydration at 450°C induced thermal migration of Ag^+ from site II to site II* and gives rise to the superior properties for air separation.*

Introduction

The separation of air for the production of nitrogen and oxygen is an important operation in the chemical processing industry. Historically, this separation has been done by cryogenic distillation. As adsorption systems have become more efficient and new, more effective sorbents have been synthesized, separation by adsorption processes [such as pressure swing adsorption (PSA), and vacuum swing adsorption (VSA)] have become increasingly competitive and are already favorable for small-to-medium-scale operations (Yang, 1997). Currently, approximately 20% of air separations are accomplished using adsorption technologies (Rege and Yang, 1997).

While it has long been known that Li^+ is among the strongest cations, with respect to its interaction with N_2 (McKee, 1964), its use was greatly increased with two recent advances. First, it was found that Li^+ ion-exchange in X-type zeolite must exceed an approximate 70% threshold before the Li^+ has any effect on the adsorptive properties of the material (Chao, 1989; Chao et al., 1992; Coe et al., 1992; Coe, 1995). Secondly, a significant increase in the N_2 adsorption capacity was seen in Li^+ ion-exchanged low-silica X (LSX) zeolite over that of the typical commercial material (Si/Al ≈ 1.25). Because of these advances, Li−LSX is now the best sorbent in industrial use for the separation of air by adsorption processes (Rege and Yang, 1997).

Examples of mixed-cation zeolites have also been given. Coe et al. (1992) reported the use of a binary exchanged X-zeolite having lithium and calcium and/or lithium and strontium ions in a ratio of 5% to 50% calcium and/or strontium and 50% to 95% lithium. This material provided for enhanced nitrogen adsorption over those of the Na−X, Li−X, and Ca−X zeolites. Chao et al. (1992) showed the use of mixed ion-exchanged A and X zeolites with lithium and an alkaline earth metal (such as Ca^{2+}, Sr^{2+}). In this case, the zeolite contained lithium and the alkaline earth cations in a mixture of 10% to 70% alkaline earth and 30% to 90% lithium. These mixed cation zeolites provided high adsorption capacity and high thermal stability. Fitch et al. (1995) reported good N_2/O_2 selectivity and N_2 capacity with mixed Li_xAl_y−X zeolite (that

Correspondence concerning this article should be addressed to R. T. Yang.

is, using Al^{3+} as the nonframework charge-compensating cation).

Silver is also known to have very strong effects on the adsorption characteristics of zeolites (Habgood, 1964; Huang, 1974; Hutson et al., 2000). Yang et al. (1996) reported the synthesis of a mixed lithium–silver (80/20) ion-exchanged X-type zeolite (Si/Al ≈ 1.25, with approximately 17 Ag^+ per unit cell), and discussed its potential use in air separation. This sorbent utilized the very strong adsorptive properties of the Ag^+ ion that provided for increased capacity over that of the Li–X while maintaining some degree of the advantageous isotherm linearity that is seen with Li–X. *Ab initio* molecular orbital calculations showed that the adsorption of nitrogen was enhanced by weak chemical interaction (through a classic π-complexation bond) with the Ag^+ cation on the zeolite framework (Chen and Yang, 1996).

Hutson et al. (1999) have reported the synthesis of mixed Li,Ag low-silica X-type zeolite in which the addition of very small amounts of silver and specific dehydration conditions resulted in enhanced adsorptive characteristics and increased energetic heterogeneity relative to those of the fully (or near fully) exchanged Li^+ zeolites. The performance of air separation by the best of these sorbents, containing, on average, only one Ag cation per unit cell, was compared to that of the fully (or near fully) Li^+-exchanged zeolite using a standard pressure-swing adsorption (PSA) cycle by numerical simulation. The results showed that the new sorbent provides a significantly higher ($>10\%$) product throughput at the same product purity and recovery, when compared to that of the fully Li^+-exchanged zeolite (Yang and Hutson, 1999).

The location of the extraframework silver in relation to the aluminosilicate framework is of primary importance for elucidating the effect of silver cations or clusters on the adsorptive characteristics of the zeolite. In this work, we have synthesized mixed Li,Ag ion-exchanged zeolites and treated these materials in ways that promote the formation of intracrystalline silver clusters. These samples were structurally characterized using Rietveld refinement of neutron powder diffraction data. The structural data were then related to the adsorptive characteristics of the mixed-cation zeolites for the gases that are of primary interest in the separation of air: N_2, O_2, and Ar.

Synthesis and Analysis

Two type-X zeolites, differing only by the Si/Al ratio, were used in this work. These were: (1) X-type zeolite with a Si/Al of 1.0 (Praxair, #16193-42, sometimes referred to as LSX, low-silica X-zeolite), and (2) X-type zeolite with a Si/Al of 1.25 (Linde, lot 945084060002). Both of these materials were binderless, hydrated powders. The unit cell for faujasite zeolites (Y, X, LSX), including conventional designation of cation sites, is shown in Figure 1.

Since the sodium form of the zeolite exchanges more readily with most cations in consideration, all zeolites were first ion-exchanged with a solution of sodium chloride in order to convert to the Na^+ form. A dilute NaOH solution was used to keep the NaCl solution at pH ≈ 9. This helps to prevent hydrolysis and breakdown of the zeolite crystal structure during the ion-exchange process. The resultant Na^+-zeolite was then used as the starting material for subsequent syntheses.

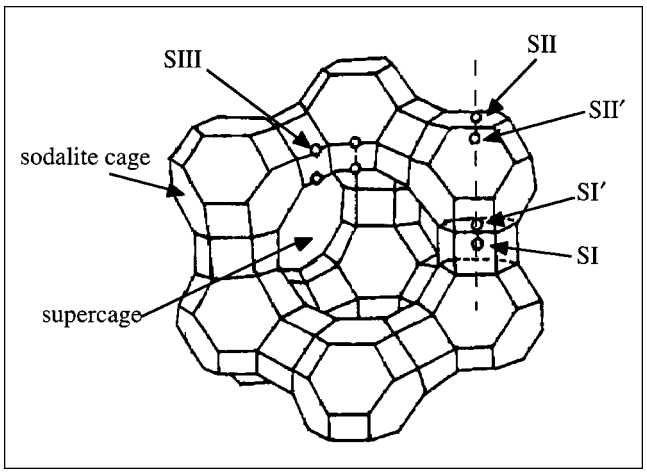

Figure 1. Unit cell, including cation sites, for faujasite zeolites.

The lithium zeolites were prepared by five consecutive static ion-exchanges using a 6.3-fold excess (over that necessary for full ion exchange) of a 2.2 M solution of LiCl. This was done in a 0.01-M solution of LiOH at a pH ≈ 9. The lithium ion-exchange solution was heated to a mild boil and then allowed to cool and settle. The solution was decanted, a fresh 6.3X LiCl solution was added, and the procedure was repeated for a total of five exchanges. After the final ion exchange, the material was vacuum filtered and washed with copious amounts of deionized water until no free ions were present in the filter water (that is, no AgCl precipitation upon treatment with Ag^+). The resulting lithium exchanged zeolites were dried overnight at 100°C in a conventional oven before being dehydrated *in vacuo* prior to measurement of adsorption isotherms.

The silver zeolites were prepared by two consecutive ion exchanges using a 0.05-M solution of $AgNO_3$. Each silver solution contained a cation content that was double that required for 100% exchange. The silver ion-exchange solution was heated to a mild boil and immediately allowed to cool and settle. As with the lithium ion-exchange, the solution was decanted, fresh $AgNO_3$ solution was added, and the procedure was repeated for a total of two exchanges. After the second ion exchange, the material was vacuum filtered and washed with copious amounts of deionized water until no free ions were present in the filter water (that is, no precipitation upon treatment with Cl^-). The silver exchanged materials were dried at room temperature and atmospheric conditions in a dark area. The resulting materials were then stored in a dark area until they were dehydrated *in vacuo* prior to analysis.

The Li_xAg_y-zeolites (which may more accurately be referred to as $Li_xNa_yAg_z$-zeolites, since ion exchange is rarely exhaustive and there is almost always some residual Na^+ present in the starting Li-zeolite) were prepared by ion exchange of a Li-zeolite (prepared as described earlier) with a 0.05-M solution of $AgNO_3$. This silver solution contained a cation content that was equivalent to the targeted amount. This is possible with silver ion-exchange because the silver cation is quickly and easily exchanged (Breck, 1984). The sil-

Table 1. Elemental Composition of the Li_xAg_y–LSX Zeolite Samples

	Sample 1		Sample 2		Sample 3		Sample 4		Sample 5		Sample 6	
Comp.	wt. %	+/−	wt. %	+/−	wt. %	+/−	wt. %	+/−	wt. %	+/−	wt. %	+/−
Al	21.38	0.88	21.19	0.87	20.80	0.85	19.45	0.81	18.37	0.75	11.91	0.49
Ag	0.00	—	0.93	0.06	3.04	0.06	9.57	0.16	15.64	0.12	55.49	0.27
Na	0.28	0.02	0.14	0.01	0.10	0.01	0.11	0.01	0.22	0.01	0.03	0.01
Li	5.59		5.21	—	4.99	—	4.76	—	3.85	—	0.00	—

Note: Lithium was measured by inductively coupled plasma—mass spectroscopy (ICP-MS). All others were measured by neutron activation analysis (NAA).

ver ion-exchange solution was heated to a mild boil and immediately allowed to cool and settle. The resulting material was vacuum filtered and washed with copious amounts of deionized water. Complete incorporation of the targeted silver ions was verified when no precipitation was observed in the filtered water upon treatment with Cl^-. These mixed-cation zeolites were then dried at room temperature and atmospheric conditions in a dark area and were stored in a dark area until they were dehydrated *in vacuo* prior to analysis.

The samples were compositionally characterized using neutron activation analysis (NAA) at the research nuclear reactor of the Phoenix Memorial Laboratory at the University of Michigan. The samples were irradiated sequentially for one minute at a core-face location with an average thermal neutron flux of 2×10^{12} N/cm^2/s. Two separate gamma-ray spectra were collected for 500 s real time for each sample using a high-resolution germanium detector. After a 13-min decay the collection was used to determine the concentrations of aluminum and silver, while data collected after 1 h and 56 min decay were used to analyze for sodium and potassium. Four replicates of NBS-SRM-1633a (coal fly ash) and silver foil were used as standard reference materials and check standards.

The samples were also analyzed for Li content using an inductively coupled plasma mass spectrometer (ICP-MS, Hewlett-Packard HP 4500). The samples were first digested in concentrated nitric acid solution at 100°C for 20 min. At the end of digestion, the samples were further diluted and filtered before the ICP-MS analyses. Results of these analyses are given in Table 1. The unit cell compositions for those analyzed samples are given in Table 2.

From this point, all samples will be identified according to the type of zeolite and the number of charge-compensating cation(s) present in a unit cell. For example Li_{86}–X refers to an X-type zeolite (with Si/Al $\approx$ 1.25) that has been fully exchanged to contain 86 Li^+ cations per unit cell. The sample $Li_{94.2}Ag_{1.1}Na_{0.7}$–LSX refers to a low-silica X-type zeolite (with Si/Al = 1.0) that contains, on average, 94.2 Li^+, 1.1 Ag^+ (or other form of Ag), and 0.7 Na^+ per unit cell, as determined from the neutron activation (NA) and ICP-MS analyses.

Structural Characterization

A separate set of mixed Li,Ag–LSX zeolites was prepared using the previously described procedure. These samples were used in the structural characterization. They were chemically characterized using neutron activation analysis (as described earlier). The unit-cell composition for each of the materials is listed in Table 3.

Neutron powder diffraction

Powder neutron diffraction data were collected for each of the samples shown in Table 3. Each of the samples was initially dehydrated under vacuum for 12 h at a prescribed temperature (as given in the sample name). The samples were exposed to atmospheric conditions during transport to the NIST Center for Neutron Research. In preparation for the diffraction experiment, approximately 10–15 mL of each sample was dehydrated under vacuum ($<10^{-5}$ torr). Each sample was heated to the temperature that was used in the prior heat treatment. Samples were heated at a rate of approximately 10°C/min, held at constant temperature for a minimum of 4 h, then were allowed to cool to room temperature. The samples were transferred to 50-mm-long and 15.6-mm-wide vanadium cans and subsequently sealed in a helium environment with low water and oxygen levels (<10 ppm). Neutron diffraction data were collected using the 32 detector BT-1 neutron powder diffractometer at the NIST Center for Neutron Research NBSR reactor (Gaithersburg, MD). Measurements were made using a Ge(311) monochromator with $\lambda = 2.0783(2)$ Å (1 Å $= 10^{-10}$ m) at ambient temperature. Data were collected over the range of 1.3–166.3° 2θ with a step size of 0.05°. The data collection time for each sample was approximately 8 h.

Table 2. Unit-Cell Composition for Each of the Li_xAg_y–LSX Samples

	1	2	3	4	5	6
atm/UC	atm/UC	atm/UC	atm/UC	atm/UC	atm/UC	atm/UC
Al	96.0	96.0	96.0	96.0	96.0	96.0
Ag	0.0	1.1	3.5	11.5	21.0	95.7
Na	1.5	0.7	0.5	0.6	1.2	0.3
Si	96.0	96.0	96.0	96.0	96.0	96.0
Li	94.5	94.2	92.0	83.9	73.8	0.0
O	384.0	384.0	384.0	384.0	384.0	384.0

Table 3. Unit-Cell Composition (in atoms/unit cell) for Each Li_xAg_y–LSX Sample Used in the Structural Determination

Component	Li–LSX atm/UC		Li_xAg_y–LSX atm/UC
Al	96	96	96
Ag	0	2.0	41.8
Na	0.2	0.7	0.2
Si	96	96	96
O	384	384	384
Li	95.8	93.3	54

Table 4. Cell Parameters and Agreement Factors for the Four Li,Ag–LSX Samples

Parameter	$Li_{95.8}Na_{0.2}$– LSX-450	$Li_{54.0}Ag_{41.8}Na_{0.2}$– LSX-450	$Li_{93.3}Ag_{2.0}Na_{0.7}$– LSX-350	$Li_{93.3}Ag_{2.0}Na_{0.7}$– LSX-450
Space group	$Fd\bar{3}(203)$	$Fd\bar{3}(203)$	$Fd\bar{3}(203)$	$Fd\bar{3}(203)$
$a = b = c$ (Å)	24.68256(27)	24.72728(33)	24.68317(30)	24.68379(28)
R_{wp} (Rietveld)	0.0513	0.0579	0.0510	0.0514
R_{Bragg} (Rietveld)	0.0424	0.0456	0.0421	0.0421
χ^2 (Rietveld)	1.352	1.456	1.233	1.319

Note: The agreement factors for each crystallographic model is compared to an ideal (Le Bail) fit. Standard uncertainties are given in parentheses. Definitions for R_{wp} and χ^2 can be found in Freeman et al. (1991) and $R_{Bragg} = \Sigma|F_o^2 - F_c^2|/\Sigma F_o^2$.

Rietveld refinement

Neutron powder diffraction data were analyzed using the Rietveld (1967) technique in conjunction with the generalized structure analysis system (GSAS) suite of Larson and Von Dreele (1986). To determine the best expected fit to the data, the Le Bail intensity extraction method was used first, in effect simulating a fit with an idealized crystallographic model (Le Bail et al., 1988). Background was fit using a Chebyshev polynomial with a variable number of terms (between 8 and 12). Lattice constants and zero-point shifts were then introduced and optimized. The peak asymmetry at low angles was treated using the model of Finger et al. (1994). Scattering factors and lengths were set to standard values for neutral atoms, as supplied in the GSAS package. Initial fractional atomic coordinates for the framework constituents in space group $Fd\bar{3}(203)$ were based upon the model determined by Feuerstein and Lobo (1998) for Li–LSX. In this refinement, since the material is an aluminum-saturated zeolite, $T(1)$ is modeled as a pure Si site and $T(2)$ is modeled as a pure Al site. The isotropic atomic displacement parameters were grouped, using one value for framework T atoms, a second value for framework O atoms, and a third for extraframework cations. Details concerning the location of extraframework cations for each material and the final stages of refinement are given in the following sections. The results of the Rietveld refinement are given in Tables 4–8. The results of the Rietveld refinements are summarized in Table 4. Positional coordinates, occupancies, and atomic displacement parameters for each sample are listed in Tables 5 and 6. Selected bond lengths (Å) and angles (degrees) are given in Tables 7 and 8. A comparison of the cation site occupancies determined in this study is given in Table 9.

$Li_{95.8}Na_{0.2}$–LSX structure

The results of the Rietveld refinement for this near fully Li-exchanged zeolite are shown in Table 4. The agreement of the experimental and the refined model were quite good ($\chi^2 = 1.352$) and agreed very well with results reported from a previous study by Feuerstein and Lobo (1998). Almost all of the lithium cations were located (93.5 of the 95.8 expected).

Table 5. Framework Atomic Parameters for the Li,Ag–LSX Samples from Rietveld Refinements of Neutron Powder Diffraction Data

Atom	Site		$Li_{95.8}Na_{0.2}$– LSX-450	$Li_{54.0}Ag_{41.8}Na_{0.2}$– LSX-450	$Li_{93.3}Ag_{2.0}Na_{0.7}$– LSX-350	$Li_{93.3}Ag_{2.0}Na_{0.7}$– LSX-450
$T(1)$*	96*g*	*x*	−0.0475(4)	−0.0485(4)	−0.0477(4)	−0.04875(29)
		y	0.1254(4)	0.1258(4)	0.1256(4)	0.1247(4)
		z	0.0392(4)	0.0368(5)	0.0397(4)	0.0373(4)
		B(Å^2)**	0.011425	0.01514	0.01299	0.01223
$T(2)$*	96*g*	*x*	−0.0528(4)	−0.0498(4)	−0.0523(4)	−0.05009(34)
		y	0.0361(5)	0.0384(5)	0.0359(5)	0.0378(4)
		z	0.1224(4)	0.1221(4)	0.1226(4)	0.1229(4)
$O(1)$	96*g*	*x*	−0.10383(2)	−0.1023(4)	−0.10306(2)	−0.10426(21)
		y	0.00341(3)	0.0021(5)	0.00381(32)	0.00367(31)
		z	0.09756(2)	0.0967(4)	0.09785(23)	0.09684(22)
		B(Å^2)**	0.0195	0.01861	0.02099	0.02023
$O(2)$	96*g*	*x*	0.00060(3)	−0.00040(33)	0.00052(30)	0.00027(26)
		y	−0.00129(3)	−0.00026(33)	−0.00148(29)	−0.00093(26)
		z	0.15314(1)	0.15355(19)	0.15358(15)	0.15300(15)
$O(3)$	96*g*	*x*	−0.02202(1)	−0.02227(19)	−0.02261(15)	−0.02232(15)
		y	0.07273(3)	0.07392(31)	0.07289(29)	0.07333(26)
		z	0.06963(3)	0.06850(35)	0.06875(28)	0.06920(27)
$O(4)$	96*g*	*x*	−0.07403(1)	−0.07414(23)	−0.07399(17)	−0.07414(17)
		y	0.08149(3)	0.0808(4)	0.08120(32)	0.08156(29)
		z	0.17121(3)	0.1717(4)	0.17176(29)	0.17165(27)

Note: Standard uncertainties are given in parentheses.
*The $T(1)$ site is completely occupied by Si; the $T(2)$ site is completely occupied by Al.
**Displacement parameters were fixed for each refinement as follows: $T(1) = T(2)$, $O(1) = O(2) = O(3) = O(4)$.

Table 6. Extraframework Atomic Parameters for the Li,Ag–LSX Samples from Rietveld Refinements of Neutron Powder Diffraction Data

Atom	Site		$Li_{95.8}Na_{0.2}$– LSX-450	$Li_{54.0}Ag_{41.8}Na_{0.2}$– LSX-450	$Li_{93.3}Ag_{2.0}Na_{0.7}$– LSX-350	$Li_{93.3}Ag_{2.0}Na_{0.7}$– LSX-450
Li(I′)	32*e*	$x = y = z$	0.0455(5)	0.0403(7)	0.0438(4)	0.0452(4)
		Occup.	0.85(4)	0.73(4)	0.890(31)	0.915(32)
		B(Å^2)	0.0415	0.02739	0.03054	0.03325
Li(II)	32*e*	$x = y = z$	0.2227(4)	0.2228(7)	0.2230(4)	0.2237(4)
		Occup.	1.06(4)	1.26(8)	1.09(4)	1.09(4)
		B(Å^2)	0.0305	—	—	—
Li(III)	96*g*	x	0.395(5)	—	0.3885(20)	0.401(4)
		y	0.399(5)	—	0.4052(19)	0.4038(33)
		z	0.1264(2)	—	0.1287(20)	0.1260(16)
		Occup.	0.337(24)	—	0.240(16)	0.264(16)
		B(Å^2)	0.1201	—	—	—
Ag(I′)	32*e*	$x = y = z$	—	0.0818(34)	—	—
		Occup.	—	0.058(11)	—	—
Ag(II′)	32*e*	$x = y = z$	—	—	0.1674(28)	0.170(6)
		Occup.	—	—	0.053(8)	0.029(7)
Ag(II)	32*e*	$x = y = z$	—	0.203(5)	—	—
		Occup.	—	0.062(22)	—	—
Ag(II*)	32*e*	$x = y = z$	—	0.2560(34)	—	0.263(5)
		Occup.	—	0.053(16)	—	0.029(7)
Ag(III)	96*g*	x	—	0.269(5)	—	—
		y	—	0.359(5)	—	—
		z	—	0.123(5)	—	—
		Occup.	—	0.053(12)	—	—
Ag(III′)	96*g*	x	—	0.3924(27)	—	—
		y	—	0.3912(28)	—	—
		z	—	0.1451(9)	—	—
		Occup.	—	0.186(7)	—	—
Al(Alum)	8*a*	$x = y = z$	—	0.125(0)	—	—
		Occup.	—	0.037(12)	—	—
O(Alum)	32*e*	$x = y = z$	—	0.174(6)	—	—
		Occup.	—	0.037(12)	—	—

Note: Standard uncertainties are given in parentheses.
Displacement parameters were fixed for each refinement as follows: Ag(I) = Ag(I′) = Ag(I″) = Ag(II′) = Ag(II′) = Ag(III) = Al(Alum) = O(Alum).

The lithium cations were located in the six-ring sites, SI′ and SII, and in the supercage 4-ring SIII site. A slight overpopulation was located at the SII site (33.9 cations); this was also the case with the study by Feuerstein and Lobo (1998).

Lithium cations in the SII site were at a distance of 1.97 Å from the closest framework oxygen (that is, Li(II)_O(2) = 1.97 Å). This short distance allows the cation to sit very deep in the face of the six-ring, effectively shielding the electrostatic energy of the cation and preventing interaction with adsorbates such as nitrogen, oxygen, and argon. The sodalite cage and double six-ring (hexagonal prism) showing the sites of lithium is shown in Figure 2.

$Li_{54.0}Ag_{41.8}Na_{0.2}$–LSX structure

The results of the Rietveld refinement for the $Li_{54.0}Ag_{41.8}Na_{0.2}$–LSX zeolite are shown in Table 4, and the agreement of the experimental and the refined model were very good ($\chi^2 = 1.456$). The lithium cations of this sample were located only in the six-ring sites, SI′ and SII. No site SIII supercage lithium cations were located. As with the near fully Li-exchanged sample, an overpopulation of Li was located at the SII site (40.3 cations). However, if one assumes that only 32 Li cations are located at this site, the total is very near the expected total value of lithium (55.4 of the expected 54.0). Because of this, it is likely that the GSAS suite, using Rietveld refinement, consistently overestimates the population of SII lithium.

Most of the silver was found in the SIII supercage sites (approximately 80% of the total found). This is an indication that the smaller lithium cations, when in competition with silver cations, prefer to occupy the six-ring sites. However, it may also be the result of the order of ion exchange. Since the low-silica X-zeolite was first ion exchanged with lithium, and then subsequently with silver, the lithium cations had the first opportunity to occupy the more energetically favorable six-ring sites. If the ion exchange was done in the opposite order, silver cation may very well have retained occupancy of the six-ring sites (for silver, those would include SI, SI′, SII′, SII, and SII*; see Figure 3).

Small amounts of silver were also located in sodalite six-ring sites (SI′, SII, and SII*). There was no silver associated with the single six-ring (SI) or inside the sodalite cage (SII′). The

Table 7. Selected Interatomic Distances (Å) and Bond Angles (°) Derived from Li,Ag–LSX Samples with Standard Uncertainties in Parentheses

Atoms	$Li_{95.8}Na_{0.2}$– LSX-450	$Li_{54.0}Ag_{41.8}Na_{0.2}$– LSX-450	$Li_{93.3}Ag_{2.0}Na_{0.7}$– LSX-350	$Li_{93.3}Ag_{2.0}Na_{0.7}$– LSX-450
Vector				
T(1)_*T*(2)	3.016(8)	3.020(9)	3.015(8)	3.011(7)
T(1)_*T*(2)	3.069(8)	3.034(10)	3.070(8)	3.036(8)
T(1)_*T*(2)	3.089(9)	3.096(10)	3.077(9)	3.095(8)
T(1)_*O*(1)	1.708(12)	1.637(9)	1.731(11)	1.639(8)
T(1)_*O*(2)	1.637(13)	1.655(14)	1.648(13)	1.648(11)
T(1)_*O*(3)	1.627(13)	1.637(9)	1.609(13)	1.630(8)
T(1)_*O*(4)	1.586(11)	1.614(9)	1.569(11)	1.607(8)
T(2)_*O*(1)	1.617(14)	1.700(9)	1.604(14)	1.706(8)
T(2)_*O*(2)	1.778(13)	1.735(10)	1.771(12)	1.736(8)
T(2)_*O*(3)	1.759(15)	1.729(9)	1.771(14)	1.730(8)
T(2)_*O*(4)	1.727(13)	1.723(9)	1.735(12)	1.723(8)
Angle				
O(1)_*T*(1)_*O*(2)	106.0(5)	110.2(8)	105.4(5)	107.9(5)
O(1)_*T*(1)_*O*(3)	108.3(7)	106.9(8)	107.0(6)	110.4(6)
O(1)_*T*(1)_*O*(4)	106.8(6)	108.8(7)	107.4(6)	108.3(6)
O(2)_*T*(1)_*O*(3)	109.5(6)	107.8(7)	109.5(6)	108.1(5)
O(2)_*T*(1)_*O*(4)	111.4(6)	111.2(6)	110.9(6)	110.2(5)
O(3)_*T*(1)_*O*(4)	114.3(6)	111.8(7)	116.1(6)	112.0(5)
O(1)_*T*(2)_*O*(2)	118.7(7)	114.4(9)	118.8(7)	116.8(6)
O(1)_*T*(2)_*O*(3)	108.1(6)	106.6(6)	107.0(6)	105.8(5)
O(1)_*T*(2)_*O*(4)	110.6(7)	108.5(8)	110.1(7)	107.6(6)
O(2)_*T*(2)_*O*(3)	105.2(6)	110.3(7)	106.8(6)	108.9(6)
O(2)_*T*(2)_*O*(4)	105.4(6)	105.2(7)	105.1(6)	107.0(5)
O(3)_*T*(2)_*O*(4)	108.3(7)	111.9(7)	108.7(7)	110.7(5)
T(1)_*O*(1)_*T*(2)	145.5(4)	148.2(6)	146.1(4)	144.98(34)
T(1)_*O*(2)_*T*(2)	127.95(33)	127.0(4)	127.73(34)	127.61(33)
T(1)_*O*(3)_*T*(2)	125.86(31)	127.5(4)	126.26(33)	127.31(33)
T(1)_*O*(4)_*T*(2)	137.7(4)	136.1(5)	137.2(4)	136.6(4)

silver site II is approximately in the plane of the six-ring. A new site, which is labeled SII* to distinguish it from the conventional SII (see Figure 3), was found in this sample. Site II* is still observed on the supercage side of the six-ring, but is shifted further away from the plane of the six-ring. Only about 70% of the expected silver was located using Rietveld refinement. One explanation for this result is that there may be reduced silver crystallites on the exterior of the zeolite. This was discussed in a previous work for near fully Ag-exchange faujasites (Hutson et al., 2000). This explanation also helps to explain the higher than expected lithium. The sodalite cage and double six-ring (hexagonal prism) showing the sites for lithium and silver occupancy is shown in Figure 3.

Fourier difference analysis indicated the presence of scattering density at the center of the sodalite cage and approximately 1.7 Å away from this site. One likely explanation for this extra scattering density is the presence of extraframework alumina in the center of the sodalite cage. This was also noted in a neutron diffraction structural analysis of near fully exchanged Ag–X and Ag–LSX zeolites. Even when carefully dehydrated, X and LSX tend to lose framework alumina through self-steaming to void spaces in the zeolite (the sodalite cage and supercage). An extraframework tetrahedral $[AlO_2]^-$ unit was added to the model with the Al^{3+} located at the center of the sodalite cage and oxygen atoms along the (111) axis. The fractional occupancies for these two atoms were constrained to be the same. Isotropic atomic displacement parameters were constrained to be the same as that of the extraframework silver.

$Li_{93.3}Ag_{2.0}Na_{0.7}$–LSX structure

These samples contained only a small amount of silver and, as a result, there was only a slight difference in the diffraction pattern as compared to that of fully Li-exchanged LSX. This makes the Rietveld refinement very difficult (Reisner, personal communication, 2000). In approaching this refinement, it was necessary to use information of the behavior of lithium and silver from the previous samples. It was also necessary to use what was already known of the behavior of silver in near fully exchanged LSX-zeolite (Hutson et al., 2000).

The results of the Rietveld refinement for the $Li_{93.3}Ag_{2.0}Na_{0.7}$–LSX zeolite (after vacuum dehydration at 350°C and at 450°C) are shown in Table 4; and the agreement of the experimental and the refined model were very good ($\chi^2 = 1.233$ for the sample heated to 350°C, and $\chi^2 = 1.319$ for the sample heated to 450°C). The overall structures of these samples are very similar to that described earlier for the $Li_{95.8}Na_{0.2}$–LSX sample. Almost all of the lithium cations were located (86.4 and 89.5 of the 93.3 expected). As with the $Li_{95.8}Na_{0.2}$–LSX sample, the lithium cations were located in the six-ring sites, SI′ and SII, and the supercage 4-ring SIII site, and a slight overpopulation was located at the SII site (34.9 cations at SII for both samples).

Table 8. Selected Interatomic Distances (Å) Derived from Li,Ag–LSX, With Standard Uncertainties in Parentheses

Atoms	$Li_{95.8}Na_{0.2}$– LSX-450	$Li_{54.0}Ag_{41.8}Na_{0.2}$– LSX-450	$Li_{93.3}Ag_{2.0}Na_{0.7}$– LSX-350	$Li_{93.3}Ag_{2.0}Na_{0.7}$– LSX-450
Li(I′)_SI	3.030(9)	3.049(10)	3.031(9)	3.044(8)
Li(I′)_Al	3.090(12)	3.009(12)	3.073(12)	3.040(10)
Li(I′)_O(3)	1.893(4)	1.890(5)	1.893(4)	1.900(4)
Li(I′)_Ag(I′)	—	1.78(14)	3.337(28)	3.32(6)
Li(II)_SI	3.044(10)	3.052(10)	3.046(10)	3.078(8)
Li(II)_Al	3.174(11)	3.148(12)	3.166(11)	3.136(9)
Li(II)_O(2)	1.970(4)	1.965(6)	1.964(4)	1.978(5)
Li(II)_Ag(II′)	—	—	2.38(12)	2.28(24)
Li(II)_Ag(II)	—	0.87(25)	—	—
Li(II)_Ag(II*)	—	1.42(15)	—	1.67(20)
Li(II)_O(Alum)	—	2.11(28)	—	—
Li(III)_SI	2.53(10)	—	2.44(5)	2.48(7)
Li(III)_Al	3.31(8)	—	3.26(5)	2.49(7)
Li(III)_Al	2.54(10)	—	2.74(4)	—
Li(III)_O(1)	2.68(12)	—	2.56(5)	2.57(8)
Li(III)_O(1)	2.57(11)	—	2.73(5)	2.41(9)
Li(III)_O(3)	2.81(5)	—	—	2.72(4)
Li(III)_O(4)	2.11(12)	—	2.00(5)	2.19(9)
Li(III)_O(4)	2.23(12)	—	2.45(5)	2.30(8)
Li(III)_Li(III)	1.53(11)	—	1.63(9)	1.92(8)
Ag(I′)_O(3)	—	2.60(10)	—	—
Ag(I′)_Ag(II)	—	3.22(20)	—	—
Ag(I′)_Ag(I′)	—	3.02(24)	—	—
Ag(I′)_Al(ALUM)	—	1.85(14)	—	—
Ag(I′)_O(ALUM)	—	2.28(19)	—	—
Ag(II′)_Ag(II′)	—	—	2.96(20)	3.2(4)
Ag(II)_Si	—	3.049(31)	—	—
Ag(II)_Al	—	3.129(32)	—	—
Ag(II)_O(2)	—	2.06(7)	—	—
Ag(II)_O(ALUM)	—	1.24(30)	—	—
Ag(II*)_O(2)	—	2.54(9)	—	—
Ag(II*)_Ag(II)	—	2.28(27)	—	—
Ag(III′)_Si	—	3.01(5)	—	—
Ag(III′)_Al	—	2.93(5)	—	—
Ag(III′)_O(4)	—	2.44(6)	—	—
Ag(III′)_Ag(III′)	—	1.18(5)	—	—
Ag(III′)_Ag(III)	—	3.20(16)	—	—
Ag(III′)_Ag(III)	—	2.26(14)	—	—
Ag(III)_Si	—	2.05(13)	—	—
Ag(III)_Al	—	1.89(13)	—	—
Ag(III)_O(1)	—	0.73(15)	—	—
Ag(III)_O(4)	—	2.48(12)	—	—
Al(ALUM)_O(ALUM)	—	2.08(27)	—	—

The mixed Li,Ag−LSX sample that had been heated to 350°C only had silver located in the SII′ location. Almost all of the silver was located (1.7 of the expected 2.0 per unit cell). The sample that had been heated to 450°C, however, had a population of 0.9 silver in both SII and SII′ (which provided the location of 1.8 of the 2.0 Ag expected). The

Table 9. Selected Interatomic Bond Angles (Degrees) Derived from Li,Ag–LSX, With Standard Uncertainties in Parentheses

Atoms	$Li_{95.8}Na_{0.2}$– LSX-450	$Li_{54.0}Ag_{41.8}Na_{0.2}$– LSX-450	$Li_{93.3}Ag_{2.0}Na_{0.7}$– LSX-350	$Li_{93.3}Ag_{2.0}Na_{0.7}$– LSX-450
O(3)_Li(I′)_O(3)	118.52(25)	119.998(14)	119.14(17)	118.70(22)
O(3)_Li(I′)_Ag(I′)	—	90.3(9)	—	—
O(2)_Li(II)_O(2)	118.95(17)	118.94(31)	118.90(17)	118.42(22)
O(2)_Li(II)_Ag(II′)	—	—	83.9(5)	82.7(5)
O(2)_Li(II)_Ag(II)	—	84.0(9)	—	—
O(2)_Li(II)_Ag(II*)	—	96.0(9)	—	97.3(5)
SI_Li(III)_Al	73.0(13)	—	70.9(12)	74.5(11)
O(2)_Ag(II)_O(2)	—	110.(6)	—	—
O(2)_Ag(II)_Ag(II*)	—	71.(6)	—	—

Table 10. Reported Site Occupancies for Extraframework Species in Li,Ag–LSX in Units of Silver/Unit Cell

Cation	$Li_{95.8}Na_{0.2}$– LSX-450	$Li_{54.0}Ag_{41.8}Na_{0.2}$– LSX-450	$Li_{93.3}Ag_{2.0}Na_{0.7}$– LSX-350	$Li_{93.3}Ag_{2.0}Na_{0.7}$– LSX – 450
Li(I′)	27.2	23.4	28.5	29.3
Li(II)	33.9	40.3	34.9	34.9
Li(III)	32.4	—	23.0	25.3
Li found	93.5	63.7	86.4	89.5
Li predicted	95.8	54.0	93.3	93.3
Ag(I′)	—	1.9	—	—
Ag(II′)	—	—	1.7	0.9
Ag(II)	—	2.0	—	—
Ag(II*)	—	1.7	—	0.9
Ag(III)	—	5.1	—	—
Ag(III′)	—	17.9	—	—
Ag Found	—	28.6	1.7	1.8
Ag Predicted	—	41.8	2.0	2.0

sodalite cage and double six-ring (hexagonal prism) showing the sites for lithium and silver occupancy is shown in Figure 3.

Adsorption

Adsorption isotherms

The adsorption isotherms were measured using a static volumetric system (Micromeritics ASAP-2010). Additions of the analysis gas were made at volumes required to achieve a targeted set of pressures. A minimum equilibrium interval of 9 s with a tolerance of 5% of the target pressure (or 0.007 atm, whichever is smaller) was used to determine equilibrium for each measurement point. The pressure transducers in the ASAP-2010 are accurate to $< 0.2\%$ for the pressure range of 0–1 atm. The sample weights were obtained using a digital

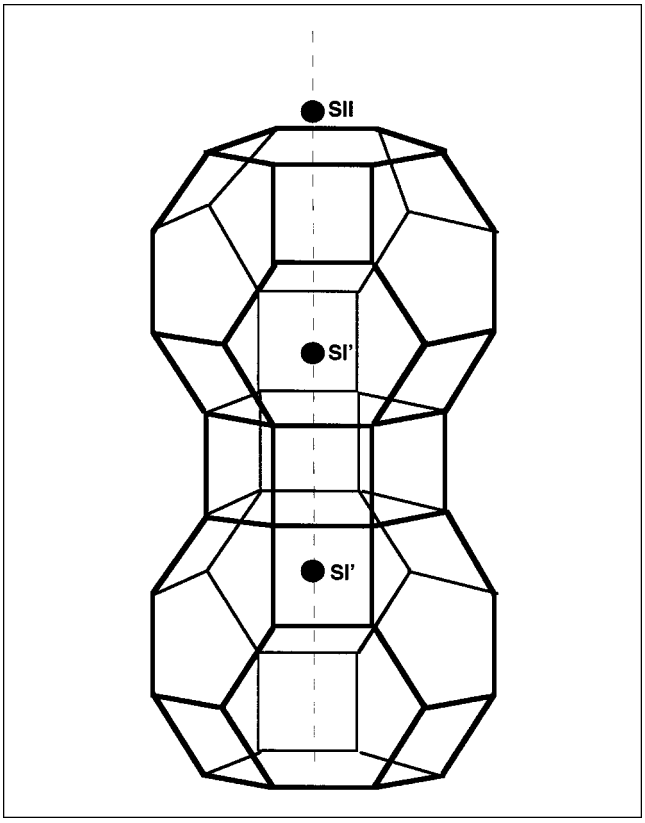

Figure 2. Position of extraframework sites in relationship to the sodalite cage in Li–LSX zeolite.

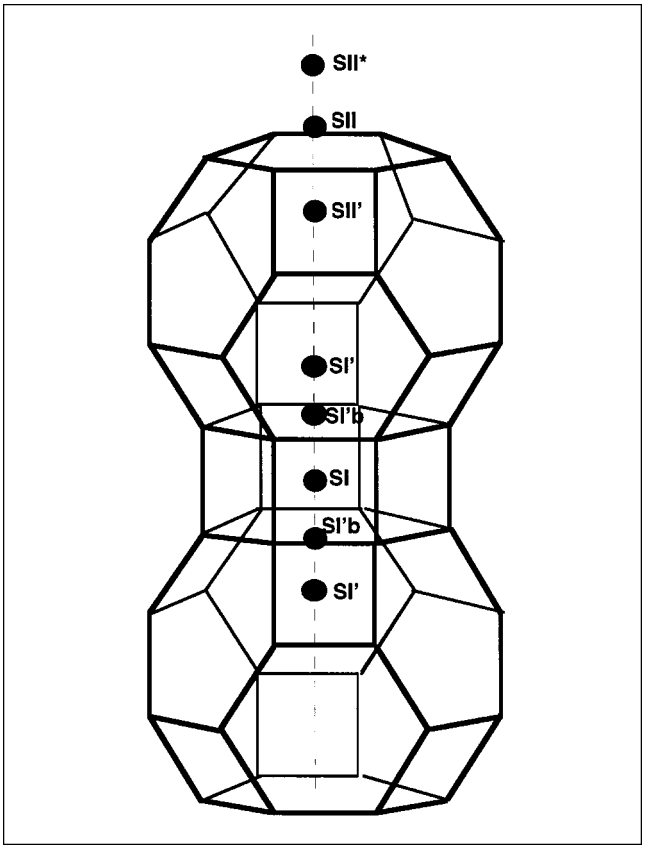

Figure 3. Position of extraframework sites in relationship to the sodalite cage in Li,Ag–LSX zeolite.

Silver was found in all sites (except SII′) for the $Li_{54.0}Ag_{41.8}Na_{0.2}$–LSX-450 (that is, dehydrated at 450°C) sample. Silver was found in the SII′ site only for the $Li_{93.3}Ag_{2.0}Na_{0.7}$–LSX-350 (dehydrated at 350°C) sample, and in the SII′ and SII* sites for $Li_{93.3}Ag_{2.0}Na_{0.7}$–LSX-450 sample.

Table 11. Conversion Factor and Cell Density for the Mixed Li_xAg_y–Zeolites

Sorbent	Conv. Factor (molec./mmol·UC)	Cell Density (g/UC)×10^{20}
$Li_{94.5}Na_{1.5}$–LSX	12.12047	2.012
$Li_{94.2}Ag_{1.1}Na_{0.7}$–LSX	12.21865	2.029
$Li_{92.0}Ag_{3.5}Na_{0.5}$–LSX	12.45768	2.068
$Li_{83.9}Ag_{11.5}Na_{0.6}$–LSX	13.26673	2.203
$Li_{7.38}Ag_{21.0}Na_{1.2}$–LSX	14.23573	2.363
$Ag_{9.7}Na_{0.3}$–LSX	21.76031	3.613
$Ag_{85.7}Na_{0.3}$–X	20.69265	3.436

laboratory balance that is accurate to ± 0.01 g. The isotherm measurements and the samples themselves were found to be highly reproducible. Helium (99.995%, prepurified), oxygen (99.6%, extra dry), nitrogen (99.998%, prepurified), and argon (99.998% prepurified) were obtained from Cryogenic Gases.

Adsorption isotherms are often reported as the amount (in mmol or vol-stp) of gas adsorbed per mass (in grams) of dehydrated sorbent. However, since there is a considerable change in the density of the resultant zeolite with the ion exchange of low-mass lithium cations for the much heavier silver cations, it is more meaningful to present adsorption data as the molecules of adsorbate in each unit cell of the sorbent, Li,Ag–zeolite. Conversion factors for this conversion are given for each of the samples in Table 11.

Figure 4 shows the N_2, O_2, and Ar adsorption isotherms, measured at 25°C, for $Li_{94.5}Na_{1.5}$–LSX after vacuum dehydration at 350°C. This zeolite is used in adsorptive air separation because of its very high N_2 capacity and very favorable N_2:O_2 selectivity (approximately 6:1 at 1 atm) as well as its N_2 isotherm linearity. Figure 5 shows the enhancement in the N_2 adsorption capacity for $Li_{94.5}Na_{1.5}$–LSX over that of $Li_{77.0}Na_{9.0}$–X. The data are shown in both mmol of adsorbate per gram of sorbent (top) and molecule of adsorbate per unit cell of sorbent (bottom).

Figure 6 shows N_2, O_2, and Ar adsorption isotherms for $Ag_{95.7}Na_{0.3}$–LSX, all measured at 25°C, after vacuum dehy-

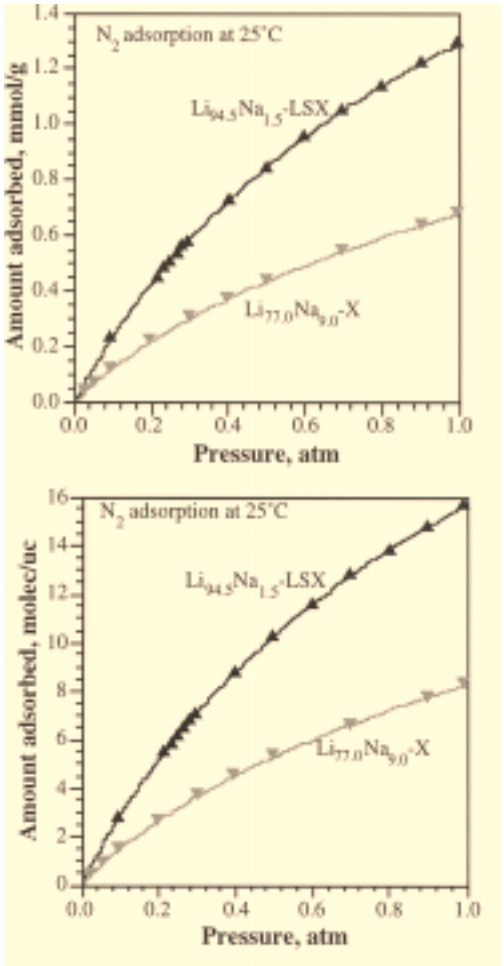

Figure 5. N_2 equilibrium isotherms measured at 25°C.

This figure shows the enhancement in the N_2 adsorption capacity for $Li_{94.5}Na_{1.5}$–LSX zeolite over that of $Li_{77.0}Na_{9.0}$–X zeolite. Both isotherms were measured after vacuum dehydration at 350°C for 4 h.

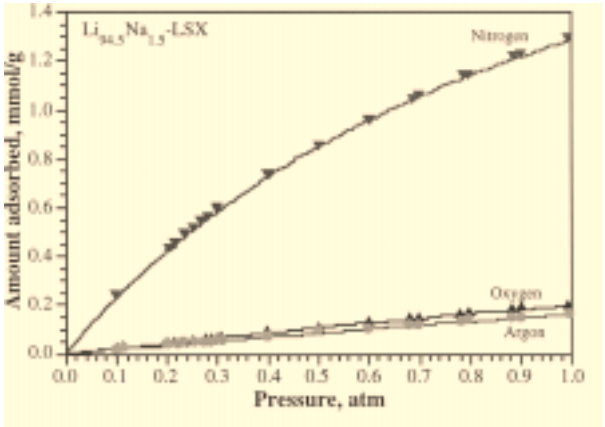

Figure 4. Single-component adsorption isotherms, measured at 25°C, for N_2, O_2 and Ar on $Li_{94.5}Na_{1.5}$–LSX after vacuum dehydration at 350°C for 4 h.

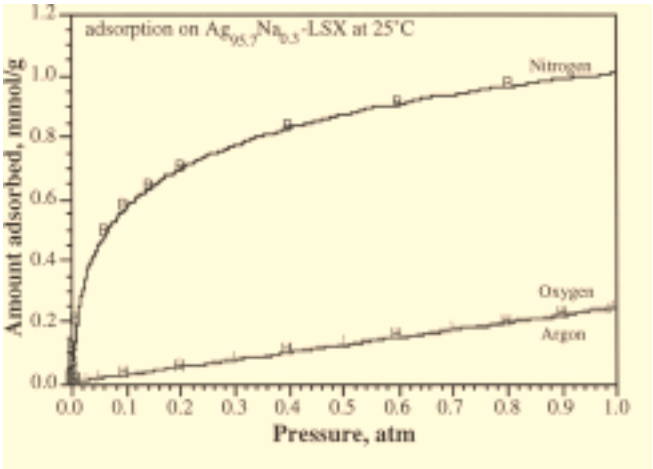

Figure 6. Single-component adsorption isotherms, measured at 25°C, for N_2, O_2, and Ar on $Ag_{95.7}Na_{0.3}$–LSX after vacuum dehydration at 450°C for 4 h.

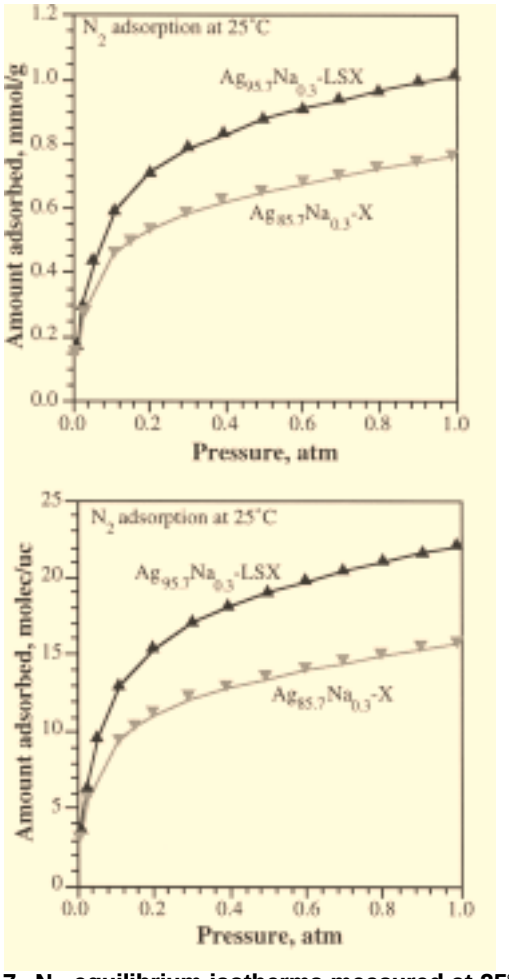

Figure 7. N_2 equilibrium isotherms measured at 25°C.

This figure shows the enhancement in the N_2 adsorption capacity for $Ag_{95.7}Na_{0.3}$–LSX over that of $Ag_{85.7}Na_{0.3}$–X. Both isotherms were measured after vacuum dehydration at 350°C for 4 h.

dration at 450°C for a minimum of 4 h. These samples were all initially gray in color, but after vacuum dehydration, turned to a deep golden yellow, indicating the formation of silver clusters (Sun and Seff, 1994). Figure 7 shows the enhancement in the N_2 adsorption capacity for $Ag_{95.7}Na_{0.3}$–LSX over that of the $Ag_{85.7}Na_{0.3}$–X. As before, the data are shown in both mmol of adsorbate per gram of sorbent (top) and molecule of adsorbate per unit cell of sorbent (bottom).

While the near fully exchanged Ag-zeolites, like their Li-zeolite analogs, have very high N_2 capacity and favorable N_2:O_2 selectivity, they are not favorable for use in adsorption-based separation. Because of the strong adsorption of N_2 at low pressure, creating a low-pressure ''knee'' in the adsorption isotherm shown in Figure 6, the working capacity (that is, the ΔQ, the change in the adsorptive capacity from the typically used adsorption pressure of 1.0 to a desorptive pressure of 0.33 atm) is very small, and the material must be exposed to very low-pressure conditions in order to increase that working capacity.

Some Ag-zeolites have been shown to have a selectivity for Ar over O_2 (Knaebel and Kandybin, 1993), and, in this work, the Ag-zeolites that had been vacuum dehydrated at 350°C also showed a selectivity for Ar over O_2. However, the Ag-zeolites that had been vacuum dehydrated at 450°C had approximately the same adsorption capacity for Ar and O_2 (as shown in Figures 4 and 6). This is likely due to increased interaction between the charged Ag-clusters (Ag^+ at SII) and the quadrupole moment of the O_2 molecule (whereas, the Ar has no quadrupole moment).

The N_2 adsorption isotherms, measured at 25°C, for Li_xAg_y–LSX zeolites after vacuum dehydration at 450°C for a minimum of 4 h are shown in Figure 8, where the amount adsorbed is given in both mmol/g (top) and molec/UC (bottom). These zeolites contained varying amounts of Ag per unit cell, ranging from zero (that is, the near fully exchanged $Li_{94.5}$-$Na_{1.5}$–LSX sample) to 21 (the $Li_{73.8}Ag_{21}Na_{1.2}$–LSX sample). This plot reveals that the incorporation of only a small amount of silver changes the adsorptive properties of the near fully exchanged $Li_{94.5}Na_{1.5}$–LSX zeolite. With increasing additions of Ag^+ (and corresponding removal of Li^+ and Na^+), the adsorption isotherms begin to take on more of the characteristics of the near fully exchanged $Ag_{95.3}Na_{0.3}$–LSX material (that is, the high ''knee'' at low pressures).

Heats of adsorption

Heterogeneity in zeolites may result from a number of causes, including a mixed population of charge-compensating cations. If the intracrystalline cation composition is mixed, sites in the vicinity of a cation will differ for each cation whether or not they occupy equivalent crystallographic positions. Further, in a mixed cation population the proportion of one cation to another can vary from one cavity to another, so that the behavior of the cavities as multiple sorption sites may vary throughout the crystal (Barrer, 1978).

The presence of energetic heterogeneity of a system can be determined by plotting the isosteric heat of adsorption vs. the amount adsorbed. Energetic heterogeneity of the system will result in a decrease in the isosteric heat of adsorption as the amount sorbed increases. For small uptakes, the isosteric heat may decrease rather strongly with the amount adsorbed. This would be an indication that there are some local intracrystalline positions where the guest molecules are preferentially sorbed more exothermally than in the rest of the intracrystalline volume.

The measurement of adsorption isotherms at different temperatures permits the calculation of the heat of adsorption as a function of surface coverage. When experimental data are reported as a set of adsorption isotherms for a particular gas-adsorbent system, the isosteric heat of adsorption is usually calculated (Bajusz and Goodwin, 1997). The isosteric heat of adsorption can be calculated from a series of isotherms by application of the Clausius-Claperyrong equation as follows:

$$\Delta H_{\text{ads}} = R\left(\frac{d\ln P}{d(1/T)}\right)_n. \qquad (1)$$

Using the data from nitrogen adsorption isotherms measured at 50°C, 25°C and 0°C (shown in Figure 9), the isosteric heats of adsorption were determined by evaluating the slope of a plot of $\ln(P)$ vs. $(1/T)$ at several coverages. The plots of

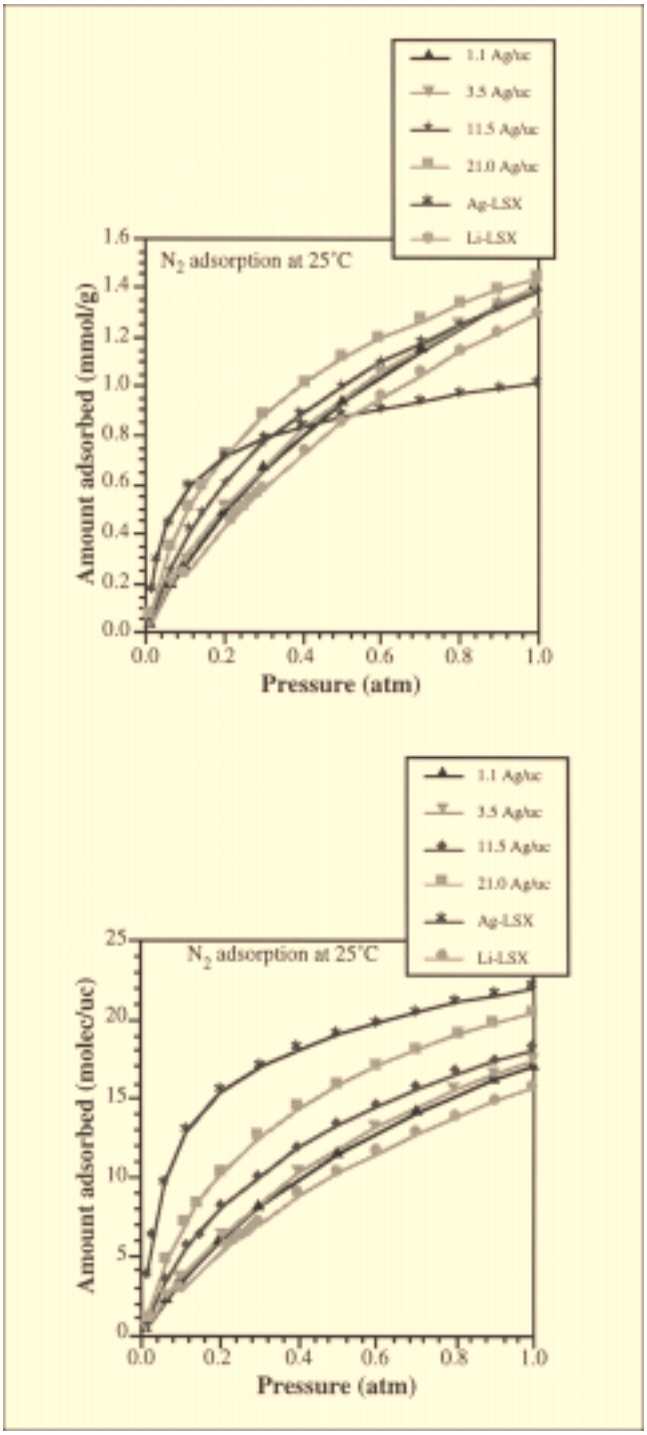

Figure 8. Equilibrium isotherms, measured at 25°C, for adsorption of N_2 on various Li_xAg_y–X-1.0 zeolites.

The amount adsorbed is given in molec/UC. This shows that the addition of increasing amounts of Ag results in a change in the general aspect of isotherm toward that of the near fully Ag^+-exchange material.

$\ln(P_{N_2})$ vs. $(1/T)$ at several coverages for $Li_{94.5}Na_{1.5}$−LSX (top) and $Li_{94.2}Ag_{1.1}Na_{0.7}$−LSX (bottom) are shown in Figure 10. The isosteric heats of adsorption at different coverages were calculated for each of these materials and are shown in Figure 11. The plots are shown as the heat of adsorption (in kcal/mol) vs. coverage in molecules of adsorbate per cavity [based on 5.7 cavities per unit cell (Breck, 1984)]. From the plots of the heats of nitrogen adsorption, one can see that the isosteric heat of adsorption for N_2 on $Li_{94.2}Ag_{1.1}Na_{0.7}$−LSX is quite high ($\approx 8$ kcal/mol) at low coverages, but immediately drops sharply to become nearly horizontal. This is very similar to that of the near fully exchanged Ag−LSX and indicates the presence of local sites where the N_2 is preferentially sorbed more strongly than at other sites within the intracrystalline volume. The heat of adsorption becomes horizontal with adsorption of approximately *one* N_2 molecule per cavity. A comparison with the same plot of the isosteric heat of adsorption for N_2 on for $Li_{94.5}Na_{1.5}$−LSX zeolite, which is essentially horizontal, shows that the energetic heterogeneity of the $Li_{94.2}Ag_{1.1}Na_{0.7}$−LSX zeolite is due entirely to the incorporation of the approximately *one* Ag per unit cell. The approximately constant heat of adsorption with increasing coverage for the $Li_{94.5}Na_{1.5}$−LSX is consistent with previously reported results (Bajusz and Goodwin, 1997), and likely indicates an energetically homogeneous surface.

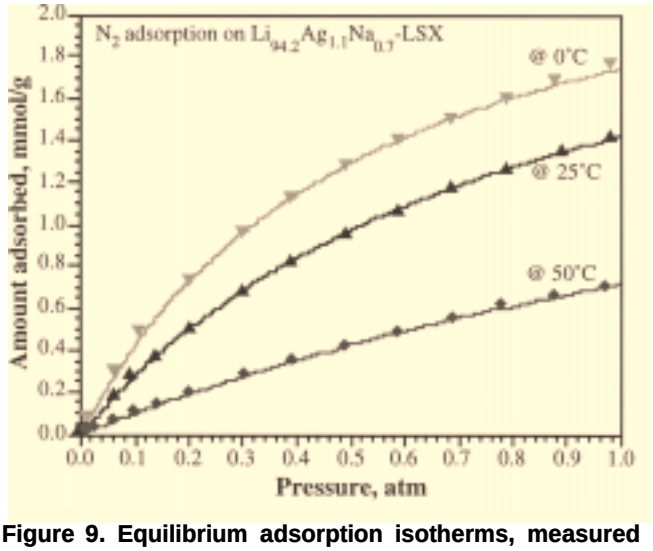

Figure 9. Equilibrium adsorption isotherms, measured at 0°C, 25°C, and 50°C, for N_2 adsorption on $Li_{94.2}Ag_{1.1}Na_{0.7}$–LSX zeolite after vacuum dehydration at 450°C.

Structural Effects on Adsorption

The adsorbate−zeolite interactions correspond to those between the adsorbing gas and the surface oxygen and charge compensating cations. In faujasite zeolites, the cations in the beta cages and the double 6-ring (hexagonal prism) are sterically inaccessible to nitrogen, and so only the supercage (SII, SII*, and SIII) cations interact with the gases of interest in air separation (N_2, O_2, and Ar). However, the electric field around these supercage cations is partially shielded by the surrounding oxygen atoms. Because of this shielding, the electrostatic and induction interactions are expected to be lower than those of an isolated ion. Further, dispersion forces

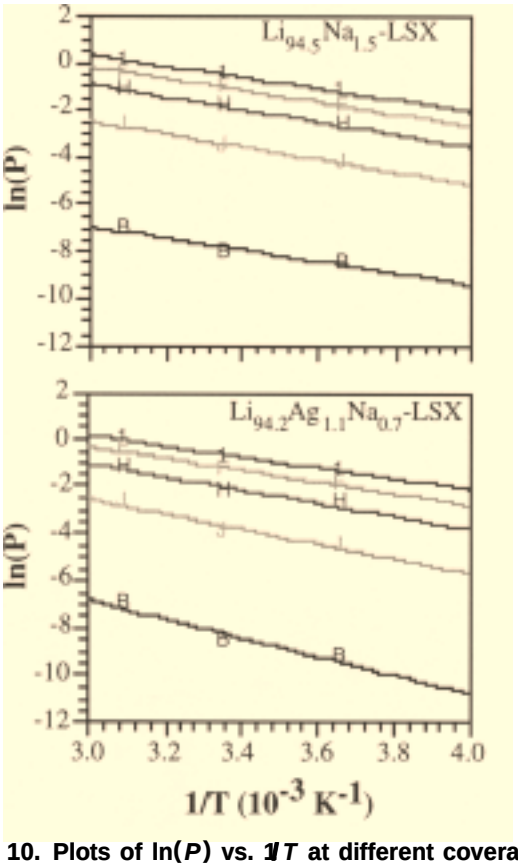

Figure 10. Plots of ln(P) vs. $1/T$ at different coverages for $Li_{94.5}Na_{1.5}$–LSX (top) and $Li_{94.2}Ag_{1.1}Na_{0.7}$–LSX (bottom).

acting on the molecule will be higher since adsorbate molecules also interact with oxygen atoms of the zeolite.

From the analysis of the structural data and the resulting effects on the adsorption of nitrogen for the near fully Ag^+-exchanged LSX (Hutson et al., 2000), one can make inferences of what are the similar effects for mixed Li,Ag–LSX. We mentioned earlier that lithium cations located in SII locations do not interact with atmospheric gases because of the short distance, and resulting shielding, to the framework oxygen. Similarly, silver cations in the SII locations, have little effect on the adsorptive properties, again, because of the shielding provided by framework oxygen (Ag–Y zeolites have very low N_2 adsorptive capacity despite having a full occupancy of SII). However, silver in SII*, are very active (Hutson et al., 2000). This helps to explain the increase in the adsorptive capacity of $Li_{94.2}Ag_{1.1}Na_{0.7}$–LSX after vacuum dehydration at 450°C over that of both the $Li_{94.2}Ag_{1.1}Na_{0.7}$–LSX after vacuum dehydration at 350°C and the $Li_{94.5}Na_{1.5}$–LSX. From the structural determinations, only the $Li_{94.2}Ag_{1.1}Na_{0.7}$–LSX zeolite contain silver in the SII* location, after vacuum dehydration at 450°C. This is supported by the fact that this is the only one of these two samples that showed the enhancement in adsorptive capacity over the near fully Li^+-exchanged LSX sample. The same sample, vacuum dehydrated at 350°C, did not show an enhancement in the adsorptive capacity, because the silver is located in the inaccessible SII′ location.

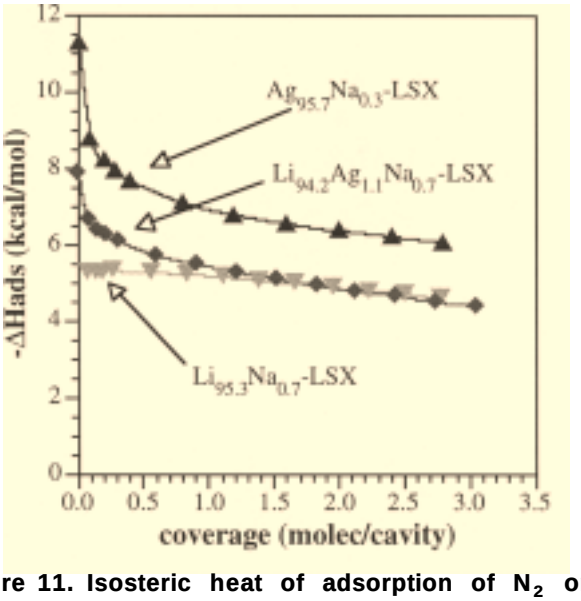

Figure 11. Isosteric heat of adsorption of N_2 on $Li_{94.5}Na_{1.5}$–LSX and $Li_{94.2}Ag_{1.1}Na_{0.7}$–LSX.

This boost in the adsorption capacity is a result of an increase in the number of SII* cations. This increase in SII* cations is a result of thermally induced silver migration from the SII′ location. This thermally induced silver migration is likely the result of a partial breakdown of the framework from autoreduction of silver with framework oxygen, as shown in Eq. 2 (Hutson et al., 2000):

$$2(Ag^+ - Z - O^-) \rightarrow 2Ag^0 + \left(\frac{1}{2}\right)O_2 + Z - O^- + Z^+. \quad (2)$$

The breakdown is not significant enough to destroy the crystallinity of the zeolite, and it is random enough to prevent its detection using X-ray or neutron diffraction. However, the breakdown likely creates an energetically unfavorable environment for the silver. As a result, silver in the SII′ then moves to the SII or SII* location. Repulsive forces (probably from silver in the SII′ location) then push the Ag into the adsorbate accessible SII* supercage position. The presence of this supercage cation (at the SII* site) results in an adsorptive surface that is energetic heterogeneous.

Acknowledgments

This work was supported by the U.S. Department of Energy under Grant DE-FG26-98FT40115. Neutron activation analyses (NAA) were conducted in the Ford Nuclear Reactor of the Phoenix Memorial Laboratory at the University of Michigan. Leah Minc of the Michigan Memorial Phoenix Project coordinated the analyses. We thank Dr. Frances Yang for performing the ICP-MS analyses. We acknowledge the support of the National Institute of Standards and Technology, U.S. Department of Commerce, for providing the neutron research facilities used in this work and a travel grant for one of the authors (N.D.H.). Drs. Barbara Reisner and Brian Toby, of the NIST Center for Neutron Research, were particularly helpful in setting up the experiments and in the use of the GSAS suite. We thank Stefan Zajic, a visiting undergraduate student from the University of Pennsylvania, for help in the synthesis of the Ag- and mixed Li,Ag-zeolites.

Literature Cited

Bajusz, I. G., and J. G. Goodwin, ''N_2 Adsorption in LiX Zeolite: Isotopic Transient Analysis,'' *Langmuir*, **13**, 6550 (1997).

Barrer, R. M., *Zeolites and Clay Minerals as Sorbents and Molecular Sieves*, Academic Press, London (1978).

Breck, D. W., *Zeolite Molecular Sieves*, Krieger, Malabar, FL (1984).

Chao, C. C., ''Process for Separating Nitrogen from Mixtures Thereof with Less Polar Substances,'' U.S. Patent No. 4,859,217 (1989).

Chao, C. C., J. D. Sherman, J. T. Mullhaupt, and C. M. Bolinger, ''Mixed Ion-Exchanged Zeolites and Processes for the Use Thereof in Gas Separations,'' U.S. Patent No. 5,174,979 (1992).

Chen, N., and R. T. Yang, ''An *Ab Initio* Molecular Orbital Study of Adsorption of Oxygen, Nitrogen and Ethylene on Silver-Zeolite and Silver Halides,'' *Ind. Eng. Chem. Res.*, **35**, 4020 (1996).

Coe, C. G., J. F. Kirner, R. Pierantozzi, and T. R. White, ''Nitrogen Adsorption with a Ca and/or Sr Exchanged Zeolite,'' U.S. Patent NO. 5,152,813 (1992).

Coe, C. G., *Access in Nanoporous Materials*, T. J. Pinnavaia and M. F. Thorpe, eds., Plenum Press, New York, p. 213 (1995).

Feuerstein, M., and R. F. Lobo, ''Characterization of Li Cations in Zeolite LiX by Solid-State NMR Spectroscopy and Neutron Diffraction,'' *Chem. Mater.*, **10**, 2197 (1998).

Finger, L. W., D. E. Cox, and A. P. Jephcoat, ''Correction for Powder Diffraction Peak Asymmetry Due to Axial Divergence,'' *J. Appl. Crystallogr.*, **27**, 892 (1994).

Fitch, F. R., M. Bulow, and A. F. Ojo, ''Adsorptive Separation of Nitrogen and Other Gases,'' U.S. Patent No. 5,464,467 (1995).

Freeman, C. M., C. R. A. Catlow, J. M. Thomas, and S. Brode, ''Computing the Location and Energetics of Organic Moelcules in Microporous Adsorbents and Catalysts: A Hybrid Approach Applied to Isomeric Butenes in a Model Zeolite,'' *Chem. Phys. Lett.*, **186**, 137 (1991).

Habgood, H. W., ''Adsorptive and Gas Chromatographic Properties of Various Cationic Forms of Zeolite X,'' *Can. J. Chem.*, **42**, 2340 (1964).

Huang, Y., ''Adsorption in AgX and AgY Zeolites by Carbon Monoxide and Other Simple Molecules,'' *J. Catalysis*, **32**, 482 (1974).

Hutson, N. D., S. U. Rege, and R. T. Yang, ''Mixed Cation Zeolites: $Li_x Ag_y$-X as a Superior Adsorbent for Air Separation,'' *AIChE J.*, **45**, 724 (1999).

Hutson, N. D., B. A. Reisner, R. T. Yang, and B. H. Toby, ''Silver Ion-Exchanged Zeolites Y, X, and Low Silica X: Observations of Thermally Induced Cation/Cluster Migration and the Resulting Effects on the Equilibrium Adsorption of Nitrogen,'' *Chem. Mater.*, (2000).

Knaebel, K. S., and A. Kandybin, ''Pressure Swing Adsorption System to Purify Oxygen,'' U.S. Patent No. 5,226,933 (1993).

Larson, A. C., and R. B. van Dreele, *GSAS: General Structure Analysis System Manual*, Los Alamos Report LAUR 86-748, Los Alamos National Laboratory, Los Alamos, NM (1986).

Le Bail, A., H. Duroy, and J. L. Fourquet, ''*Ab Initio* Structure Determination of $LiSbWO_6$ by X-Ray Powder Diffraction,'' *Mater. Res. Bull.*, **23**, 447 (1988).

McKee, D. W., ''Separation of an Oxygen-Nitrogen Mixture,'' U.S. Patent No. 3,140,933 (1964).

Rege, S. U., and R. T. Yang, ''Limits for Air Separation by Adsorption with LiX Zeolite,'' *Ind. Eng. Chem. Res.*, **36**, 5358 (1997).

Rietveld, H. M., ''Line Profiles of Neutron Powder-Diffraction Peaks for Structure Refinement,'' *Acta Crystallogr.*, **22**, 151 (1967).

Sun, T., and K. Seff, ''Silver Clusters and Chemistry in Zeolites,'' *Chem. Rev.*, **94**, 857 (1994).

Yang, R. T., *Gas Separation by Adsorption Processes*, Imperial College Press, London, and World Scientific, River Edge, NJ (1997) (reprinted from Butterworth, Boston, 1987).

Yang, R. T., Y. D. Chen, J. D. Peck, and N. Chen, ''Zeolites Containing Mixed Cations for Air Separation by Weak Chemisorption-Assisted Adsorption,'' *Ind. Eng. Chem. Res.*, **35**, 3093 (1996).

Yang, R. T., and N. D. Hutson, ''Lithium Based Zeolites Containing Silver and Copper and Use Thereof for Selective Adsorption,'' U.S. Patent Pending, U. S. Patent Office No. 60/114, 371 (1999).

Manuscript received Feb. 24, 2000, and revision received May 15, 2000.